Initial Atmospheric Corrosion of Zinc Exposed to Formic Acid, Investigated by in Situ Vibrational Sum Frequency Spectroscopy and Density Functional Theory Calculations†

ARTICLE *in* THE JOURNAL OF PHYSICAL CHEMISTRY C · SEPTEMBER 2008

Impact Factor: 4.77 · DOI: 10.1021/jp805582h

Initial Atmospheric Corrosion of Zinc Exposed to Formic Acid, Investigated by in Situ Vibrational Sum Frequency Spectroscopy and Density Functional Theory Calculations†

Jonas Hedberg,*,‡ Jaime Henriquez,§ Steven Baldelli,*,∥ C. Magnus Johnson,⊥ and Christofer Leygraf‡

Department of Chemistry, Division of Corrosion Science, Royal Institute of Technology, Drottning Kristinas v. 51, SE-100 44 Stockholm, Sweden, Chemistry and Natural Resources Institute, Talca University, 2 Norte 685, Casilla 721, Talca, Chile, Department of Chemistry, University of Houston, Houston, Texas 77204-5003, and Department of Chemistry, Surface Force Group, Royal Institute of Technology, Drottning Kristinas v. 51, SE-100 44 Stockholm, Sweden

Received: June 24, 2008; Revised Manuscript Received: August 13, 2008

Vibrational sum frequency spectroscopy (VSFS) and ab initio density functional theory (DFT) calculations of formic acid on ZnO/Zn have been performed in order to understand the first step of atmospheric corrosion on zinc initiated by formic acid. In addition, infrared reflection absorption spectroscopy (IRAS) has been employed to complement the surface sensitive VSFS results to identify the corrosion products. Oxidized polycrystalline zinc samples were exposed to 120 ppb formic acid in either humid or dry air where, the formic acid adsorption on ZnO/Zn is observed to have a low dependence on the humidity, as deduced by VSFS. Formate is formed on the surface in both dry and humid air and stabilized in configuration after about 90 min exposure in 120 ppb formic acid as seen in the VSFS results. This is evidenced by the occurrence of the CH and symmetric COO^- vibrations of the formate ion. The DFT calculations support the VSFS results, showing a coordination of the formate to zinc ions without participation from water molecules.

Introduction

Atmospheric corrosion is a costly and complex form of corrosion that involves chemical, electrochemical, and physical processes in three phases (solid, liquid, and gas) and three interfaces (solid/liquid, liquid/gas and solid/gas). Since the development of interface sensitive spectroscopic techniques, it has become possible to perform molecular in situ analyses of the interfaces involved under ambient atmospheric pressure conditions.[1−3] From these studies a conceptual framework has evolved to describe the initial stages of atmospheric corrosion. A crucial step here is the coordination of a proton or a ligand to the corroding surface, as a precursor to metal ion dissolution from the oxide-covered metal surface.[3]

Formic acid is regarded as one of the most important indoor corrosion accelerators. It is emitted from wooden objects, adhesives, and plastics. Field exposures have shown that formic acid plays an important role in indoor corrosion.[4] For example, the indoor corrosion of lead in organ pipes have been seen to be greatly affected by formic acid.[5,6] Indoor formic acid concentrations have been found to be around 20 ppb.[7]

Aims of the Study. This study is part of a larger effort to describe the initial atmospheric corrosion of zinc and copper exposed to small organic acids by studying all the interfaces that take part in the process. Earlier studies include a vibrational sum frequency spectroscopy (VSFS) study of formic acid at the air/water interface.[8] It was observed that the formic acid is still in its protonated state at this interface and forms an ordered structure at the air/water interface, where the CH group is directed toward the vapor phase and the COOH into the bulk liquid. At high concentrations of formic acid, the air/water interface is dominated by formic acid and no water is observed. This can be explained by the fact that there are fewer water molecules in the solution at high formic acid concentrations. A similar study has also been performed on acetic acid,[9,10] where it was observed that acetic acid is more surface active at the air/water interface, while for both acids, no ionized species were observed at the interface.

Infrared spectroscopy (IRAS), which probes thin films on metals, has been used to study zinc exposed to formic acid.[2] Here it was concluded that formate ions are present on the surface and that a high relative humidity increases the rate of formation of the zinc formate. Also, work on zinc and copper exposed to acetic acid have been performed[2,11,12] and displays slower corrosion kinetics than formic acid on both metals.

For studying the interface between the substrate and the thin liquid film on the surface, in situ surface sensitive VSFS and grazing incidence infrared reflection absorption spectroscopy (IRAS) experiments, along with ab initio density functional theory (DFT) calculations have been employed. VSFS is used to elucidate in what form the formic acid adsorbs and also to gain information about the structuring and ordering of the adsorbed species. The role of the DFT calculations is to provide information on adsorption sites for the formate ion and its interaction with the ZnO substrate and water molecules.

Growth of Corrosion Products and Substrate Heterogeneity. The simplest model for the growth of thin films of corrosion products is as a uniform layer-by-layer type of growth, but in atmospheric corrosion this model is generally not valid.[13,14] There are many reasons for this, such as the use of polycrystalline material, oxides, roughness of the substrate and rate of

† Part of the special section "Physical Chemistry of Environmental Interfaces".

* To whom correspondence should be addressed. Fax: +46 8 208284 (S.B.). E-mail: jhed@kth.se (J.H.); sbaldelli@uh.edu (S.B.).

‡ Division of Corrosion Science, Royal Institute of Technology.

§ Talca University.

∥ University of Houston.

⊥ Surface Force Group, Royal Institute of Technology.

10.1021/jp805582h CCC: $40.75
Published on Web 10/01/2008

film formation, to name a few. First, the samples used are not homogeneous. In this work a polycrystalline zinc sample is used which, is inherently inhomogeneous. In addition, after the prepared zinc is exposed to air, a thin oxide/hydroxide layer is formed on the substrate which is not uniform.[13,14] The corrosion process in itself favors a heterogeneous surface. There are anodic regions, the zinc ions are released, and cathodic sites, where the electrons are consumed by forming hydroxide ions.[15] Thus as the corrosion progresses, a distribution of the corrosion products are expected as it reflects the heterogeneous substrate.

In this study, it is observed that formic acid adsorbs onto zinc oxide in an atmosphere of both humid and dry air and zinc formate species are observed on the surface. There is a marked difference between the time evolution of the surface species and the thin film of more bulk-like zinc formate. The surface zinc formate structure stabilizes within ~90 min exposure to both humid and dry air, while the thin film of zinc formate continues to grow beyond this point.

Theory

Vibrational Sum Frequency Spectroscopy (VSFS). VSFS is a nonlinear laser spectroscopic technique which is inherently surface sensitive.[16,17] The VSFS signal is generated in noncentrosymmetric environments, such as the phase boundary between two centrosymmetric media, therefore, VSFS is able to probe any interface accessible by light. Two incident beams impinge on the surface, one in the visible (532 nm) and the other in the infrared (IR) region, which overlap in space and time at the interface. The IR frequencies are scanned while the visible is kept constant, creating a photon in the process which is the sum of the frequencies of the two incoming beams. Increase in intensity of the sum frequency beam corresponds to a resonance between the infrared beam and a vibrational mode at the surface.

The intensity of the sum frequency light depends on the intensity of the incoming beams, I_{IR} and I_{Vis}, and the second order nonlinear susceptibility, $\chi^{(2)}$.

$$I_{SF} \propto |\chi^{(2)}|^2 I_{IR} I_{Vis} L_{SF} K_{IR} K_{Vis} \quad (1)$$

Here L_{SF}, K_{Vis} and K_{IR} are the Fresnel factors. The second order nonlinear susceptibility $\chi^{(2)}$ includes the information about the molecules at the surface. $\chi^{(2)}$ can be divided into two parts, $\chi^{(2)}_{NR}$, which originates primarily from the substrate, as well as the resonant part, $\chi^{(2)}_{R}$, which contains the vibrational resonant contribution.

$$\chi^{(2)} = \chi^{(2)}_{NR} + \sum_n \chi^{(2)}_{R,n} \quad (2)$$

where n is the number of vibrational resonances. $\chi^{(2)}_{R}$ depend on the orientational average of the molecules at the interface, therefore only molecules with a net orientation are observed in VSFS.

Four different polarization combinations of the three beams involved can be employed to deduce the $\chi^{(2)}_{R}$ tensor elements (ppp, ssp, sps, and pss). The polarization combination used herein is ppp (p-polarized sum frequency beam, p-polarized visible beam and p-polarized IR beam). p-polarized light refers to light with polarization parallel to the plane of incidence, as opposed to s-polarized light, which is polarized perpendicular to the same plane. The sps and pss polarization combinations give no sum frequency spectra for metal surfaces, due to the fact that the infrared beam intensity is zero at the metal surface for s polarized light.[18] Further, ssp spectra for zinc exposed to formic acid did not show any vibrational resonances, giving no additional information.

Experimental Section

Sample Preparation and Exposure. Polycrystalline zinc (Goodfellow, 99.99%) was used as sample-material. The zinc samples were rectangular with an area of 2 cm^2 and a thickness of 1 mm. They were abraded with SiC grit paper, from 500 mesh in steps down to 4000 mesh, using water as lubricant. Diamond polishing was subsequently applied with particle sizes 3 μm, 1 μm and, finally, 0.25 μm. In order to remove residual diamond particles, each sample was sonicated in ethanol for 5 min between each diamond polishing step. After diamond polishing it was sonicated two times in pure ethanol and finally it was rinsed with pure water, dried with nitrogen gas and inserted into the sample cell. There it was kept in dry N_2 gas and a spectrum before exposure was collected.

The system for generating the corrosive air has been described in detail in a previous publication.[1] Here it will be described only briefly. The corrosive air was generated by mixing three different sources; one dry, one humid, and one dry containing formic acid. The dry air was generated by a Zander KEA adsorption dryer, and was also filtered with a Labclear filter. The water was obtained from a Millipore RiOs-8 and Milli-Q PLUS purification system, filtered through a 0.2 μm Millipak filter. The resistivity was 18.2 $M\Omega \cdot cm^{-1}$. The formic acid was obtained by a permeation tube (Vici Metronics) calibrated so that the concentration of formic acid was 120 ppb at the flow rates of this experiment. These three flows were mixed so that the relative humidity (RH) could be controlled between 0 and 100% and the flow velocity was ~4 cm/s along the sample surface, assuming a laminar flow. This flow rate is equivalent to a wind velocity of stagnant indoor conditions. The total flow rate was 1200 cm^3/min. Relative humidity was measured with a Hygroclip probe (Swema, Sweden) with an accuracy of ±1.5% RH. Exposures were conducted at controlled temperatures (19 ± 1.5 °C) and repeated as triplicates.

The experiments were performed in a Teflon cell in which the corrosive air entered from the top and was split up so that it was not directly hitting the sample. There are two symmetrically placed outlets for the cell, positioned three mm above the sample. The sample cell is depicted in Figure 1. This is a similar geometry as previously used for in situ atmospheric corrosion experiments based on IRAS and the quartz crystal microbalance.[1]

Vibrational Sum Frequency Spectroscopy (VSFS). The VSFS setup has been described in detail in a previous publication.[9] In short, an Ekspla Nd:YAG picosecond laser with an output wavelength of 1064 nm, 24 ps long pulses and a repetition rate of 20 Hz was used to pump an optical parametric generator/optical parametric amplifier (OPG/OPA) from Laservision. In the OPG/OPA an infrared and a visible beam are generated. The output energy from the OPG/OPA in the CH region (2800−3000 cm^{-1}) was ~300 and 40 μJ for frequencies lower than 2000 cm^{-1}. The infrared beam was scanned with a speed of 1 cm^{-1}/s. The energies of the infrared and visible beams were measured and used for normalization of the generated sum frequency intensity. For experiments in the CH-region, the IR beam was unfocused with a diameter of 2 mm and the visible beam was 1.5 mm in diameter in order to avoid sample damage. In the experiments below 2000 cm^{-1}, where the IR energy was considerably lower, the beam was softly focused 2 cm behind the sample with a +200 mm BaF_2 lens.

The linearity of the detector was checked by changing the intensity of the IR and visible beams independently, checking that the normalized sum frequency response was proportional to different energies of the incoming beams.

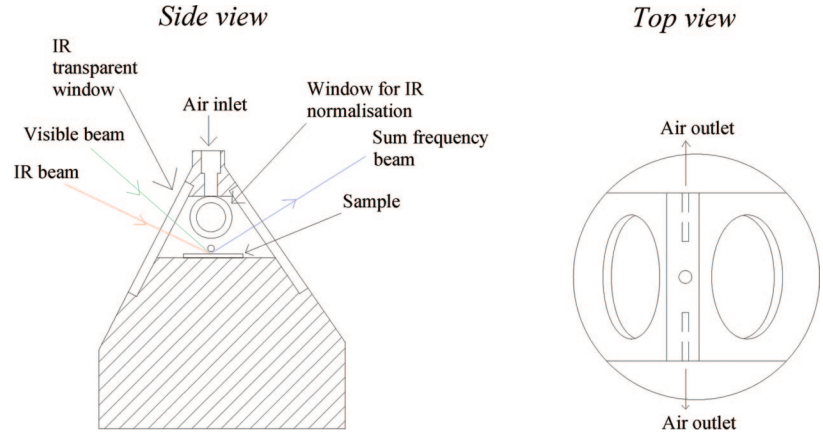

Figure 1. VSFS sample cell. A CaF_2 window was used for the incoming beams when measuring in the CH region and a BaF_2 in the carbonyl region. The cell is constructed from Teflon. The gas enters from the top and is split up so it does not hit the sample directly.

The intensity, I_{SF}, of the VSFS spectra was fitted to a Lorentzian function with Origin software (eq 3). To account for experimental scattering of the data, the instrumental weighting option was used in the error analysis.

$$I_{SF}(\omega_{IR}) \propto \left| \chi^{(2)}_{NR} + \sum_n \frac{A_n}{\omega_n - \omega_{IR} - i\Gamma_n} \right|^2 \quad (3)$$

Here n is the number of vibrational resonances in the spectrum, ω_n is the peak wavenumber of the resonances, A is the amplitude of the vibration, ω_{IR} is the infrared frequency of the light and Γ_n the damping constant. $\chi^{(2)}_{NR}$, which is a complex number, is the nonresonant background that originates mostly from the substrate.

Infrared Reflection Absorption Spectroscopy (IRAS). The setup for the IRAS experiments has been described in detail in a previous publication.[1] The experiments were performed in situ using a Digilab FTS 40 Pro FTIR spectrometer. The beam is directed to an external chamber with CdTe windows. The beam is p-polarized and strikes the sample at grazing incidence (around 78° from the surface normal). The detector is a nitrogen-cooled mercury cadmium telluride (MCT) detector. The resolution was 4 cm^{-1} and 1024 scans were collected for each spectrum. The zinc samples were kept in dry air for 30 min and a background spectrum was collected. After this the sample was put in humid air (90% RH) for 30 min and another background spectrum was collected. Then the sample was exposed, and the collected spectra were corrected against the appropriate background spectrum. In this way, the spectra were obtained in absorbance units, $-\log(R/R_0)$, where R is the reflectivity of the sample and R_0 the reflectivity of the background. Using this method for background subtraction, the absorption losses of water in the chamber could be accounted for. For obtaining the amplitudes of the vibrational resonances, a standard Lorentzian function was used to fit the spectra.

Density Functional Theory (DFT) Calculations. All quantum mechanics calculations were performed with the Gaussian03 package.[19] In all cases, a full structure optimization was carried out at the density functional theory level of calculation, with the hybrid exchange,[20] correlation functional B3LYP,[21] and the Land2dz pseudopotential basis set. The pseudopotential methods[22] can reduce the formal M^4 dependence of the Coulomb and exchange operators in the basis set representation.

A zinc oxide surface was modeled as a cluster concept.[23] This is a group of atoms in the virtual space with a special geometry, enabling the atoms involved to have chemical properties similar to a real zinc oxide surface. This was constructed to preserve the geometry of ZnO (100), where the final geometry was frozen for a correct representation. A real ZnO surface is hydroxylated when exposed to a humidified atmosphere.[24] This was simulated during the calculations by an optimization of hydrogen atoms over the frozen cluster zinc oxide surface representation.

The solvent (water) was simulated as two explicit water molecules and with the polarization continuum model (PCM) model, in which the cavity is created via a series of overlapping spheres, initially devised by Tomasi and co-workers.[25−33] The PCM solvent model calculates the molecular free energy in solution as the sum over three terms: $G_{sol} = G_{es} + G_{dr} + G_{cav}$. These components represent the electrostatic (es) and the dispersion−repulsion (dr) contributions to the free energy, and the cavitation energy (cav). All three terms are calculated using a cavity defined through interlocking van der Waals spheres centered at atomic positions. In a continuum model of solvation, such as the PCM model, the solvent is a continuum medium without structure that is polarized by solute effects. Having an electrostatic response it causes a change in the energy, in the optimized structure, and in other properties of the solute. Hence, in order to include water molecules as solute and in this way perform a characterization of the interaction between water, surface and formate, it was necessary introduce explicit water molecules. That protocol is called an explicit−implicit model, i.e., the Tomasi cavity model plus an explicit solvent water model.

The zinc oxide cluster representation was kept frozen and all the remaining atoms, including the hydrogen atoms of the hydroxylated layer, were fully optimized during the interaction between the surface, water, and formate ion.

The calculations were performed on a monolith computer cluster of the National Supercomputer Center in Sweden,[34] SGI-Altix450 server and "Q", a Dell - PowerEdge SC1860 machine, of the Bioinformatics and Molecular Simulation Center and Chemistry Institute of Natural Resources, respectively, in Talca, Chile.[35]

The visualization of the quantum chemistry results were accomplished by Gaussview4.1.2[36] and VMD 1.8.6 codes.[37]

Results and Discussion

Vibrational Sum Frequency Spectroscopy. First, the VSFS spectra obtained after different exposure times of formic acid in humid (90% RH) or dry air are considered. The purpose of this experiment is to observe the time-dependent adsorption of formic acid to the surface, and identify its state. Note, however, that dry air here does not mean totally water-free. The resolution

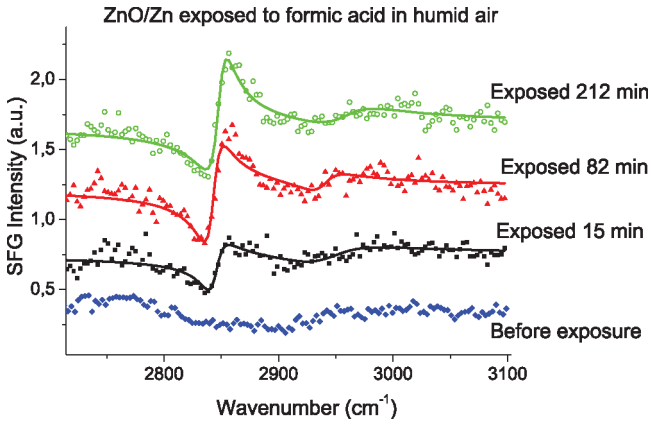

Figure 2. VSFS spectra of ZnO/Zn exposed to formic acid in 90% RH for different exposure times. ppp polarization. The spectra have been offset for clarity. Solid lines are fits to the data.

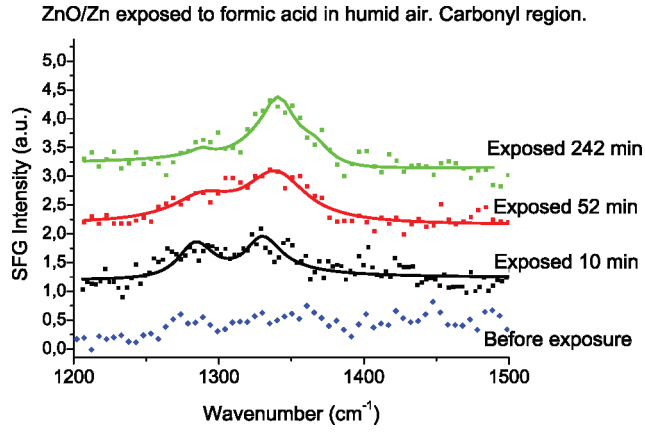

Figure 3. VSFS spectra of ZnO/Zn exposed to formic acid in 90% RH. ppp polarization. The spectra have been offset for clarity. Solid lines are fits to the data.

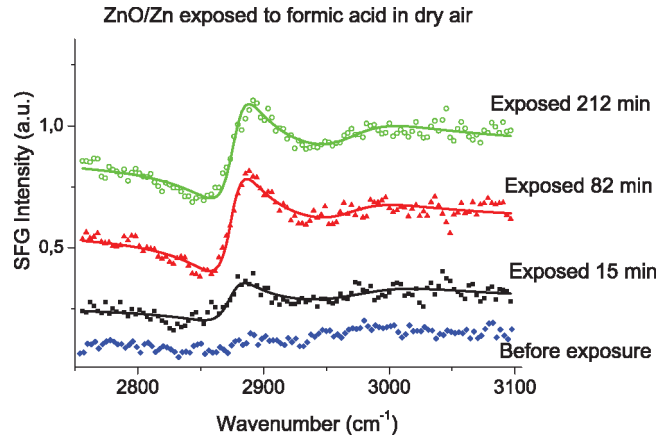

Figure 4. VSFS spectra of ZnO/Zn exposed to formic acid in 0% RH for different exposure times. ppp polarization. The spectra have been offset for clarity. Solid lines are fits to the data.

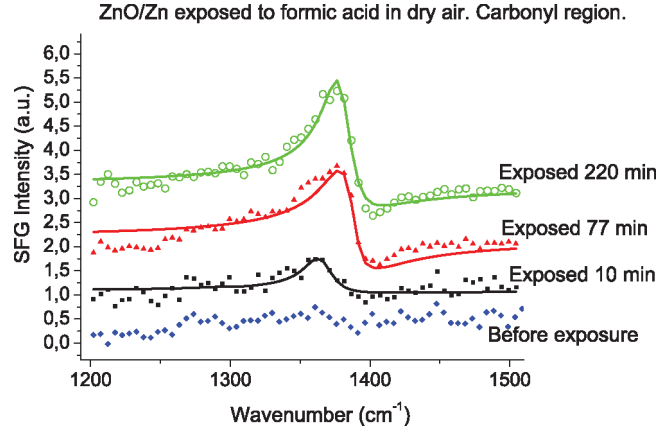

Figure 5. VSFS spectra of ZnO/Zn exposed to formic acid in 0% RH. ppp polarization. The spectra have been offset for clarity. Solid lines are fits to the data.

of the humidity meter, in addition to the fact that the experiments were conducted at atmospheric pressure, in which there is always a partial pressure of water present, indicates that there is still some water on the surface in what is defined as "dry" in this work. However, the difference between dry and humid conditions is large. 90% RH corresponds to the adsorption of more than 10 equivalent monolayers of water, while at dry conditions, the coverage is well below one monolayer.[38]

Figures 2 and 3 show the time-dependent VSFS spectra in the CH− (2800−3100 cm^{-1}) and carbonyl− (1200−1500 cm^{-1}) stretching regions, respectively, for ZnO/Zn exposed to formic acid in humid air. In Figure 2, a vibrational resonance is seen at 2850 cm^{-1}, and also a very weak peak at 2960 cm^{-1}. In the carbonyl region, Figure 3, there is a peak at 1345 cm^{-1} and also a peak at 1280 cm^{-1}. In Figures 4 and 5, the time evolution of VSFS spectra for ZnO/Zn exposed to formic acid and dry air in the CH and carbonyl stretching regions are shown, respectively. Figure 4 displays a peak at 2880 cm^{-1} and a weak peak at 2960 cm^{-1}. In Figure 5 there is a peak at 1385 cm^{-1}.

Overall the spectra in Figures 2−5 show a similar trend. One strong peak is observed, which increases intensity until a certain exposure time after which the growth stops. The solid lines are fits to the data, using the Lorentzian function (equation 3). The spectra collected before exposure show essentially no features. The assignments for the observed peaks in Figures 2−5 will be discussed below. The spectra in Figures 2−4 were fitted with two peaks, and in Figure 5 one peak was used.

ZnO/Zn exposed to formic acid is a system which has been the subject of several investigations.[2,32,39−42] Exposures have been performed both in vacuum on single crystalline ZnO surfaces[39,40,42] and at atmospheric pressure conditions on polycrystalline substrates.[2,43,44] It has been concluded that formate is the main species on the surface when Zn is exposed to gas phase formic acid at room temperature.[44] Despite this conclusion, a large range of peak frequencies for the CH and COO^- stretching vibrations of the formate ion have been reported, as seen in Table 1. This is probably because of the sensitivity to its precise environment and bonding, as suggested by theoretical studies where it was shown that the vibrational frequencies shift for different coordinations.[32] In addition, the previous studies have been conducted using a variety of techniques and conditions, which also influences the observed peak frequencies. Similarly, there are quite significant differences in vibrational peak frequencies when using different single crystal orientations of ZnO.[39] In all, it is evident that the CH and COO^- peak frequencies vary between the studies, and there is no single reference that matches the frequencies observed in the VSFS experiments performed in this work. However, the assignments of the peaks will be made so that the peaks at 2850 and 2880 cm^{-1} correspond to the CH-stretching vibration of the formate and the peaks at 1340 and 1385 cm^{-1} correspond to the symmetric COO^- vibration of formate. The vibrations in the CH and carbonyl regions are correlated, meaning that in both regions, peaks corresponding to formate are observed strength-

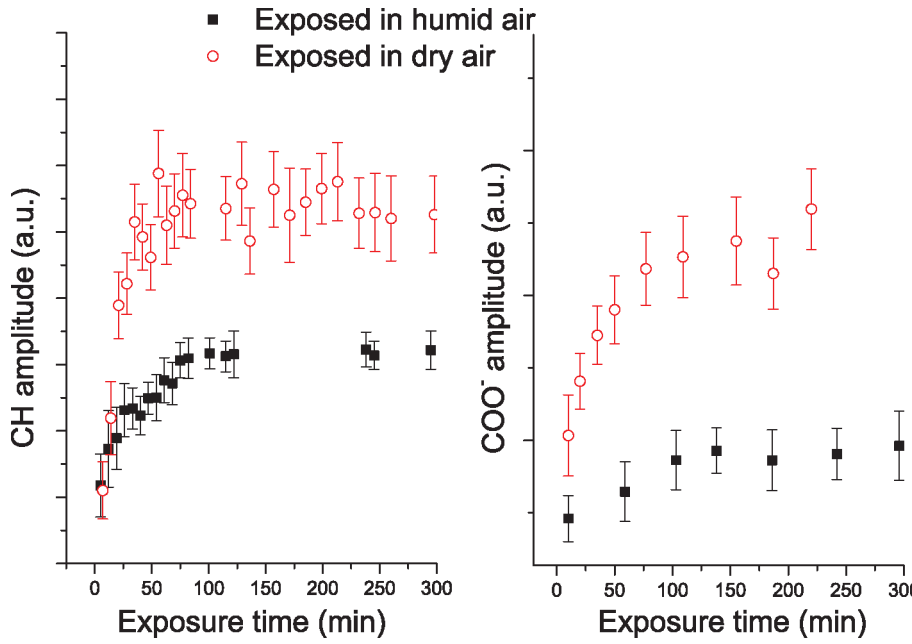

Figure 6. Fitted VSFS amplitudes of the CH and symmetric COO^- peaks of ZnO/Zn exposed to either humid or dry air. The absolute amplitudes are not comparable between the different experiments, therefore the *y*-axis scale only shows arbitrary units.

TABLE 1: Vibrational Frequencies for Formate and Formic Acid Species on ZnO/Zn

vibrational mode	ZnO/Zn, VSFS, this work (cm^{-1})	ZnO/Zn, IRAS[2] (cm^{-1})	ZnO(0001),HREELS[42] (cm^{-1})	ZnO(10$\bar{1}$0)HREELS[39] (cm^{-1})	ZnO powder, IR[47] (cm^{-1})	Formic acid, IR[45]
υ(CH)	2850 2880 2960	2860	2939	2895	2870	2958
$\upsilon_s(COO^-)$	1340 1385	1345	1387	1363	1369	
υ(C−O)	1280					1255 1224

ening the assignments. These observed frequencies in the current work are in the range of the reported values for these peaks (Table 1). The weak peaks at 1280 and 2960 cm^{-1} are of C−O and C−H type and may be associated with formic acid.[45,46]

The fact that formate is present in dry as well as humid air conditions is not a surprise since it has been observed previously.[42,44] Zn and ZnO have the ability to deprotonate formic acid, and thereby generate a formate ion and a hydrogen ion. The reaction is spontaneous and results in a formate ion bonded to the ZnO/Zn substrate and an OH group formed by the hydrogen ion produced in the deprotonation. The rate of the decomposition is independent of the pressure of the formic acid.

Growth Kinetics of VSFS and IRAS Peaks. Figure 6 displays the time-dependent amplitudes of the CH and symmetric COO^- vibrations of the formate after exposures in both dry and humid air containing formic acid. The amplitudes were extracted from the spectra after fitting with eq 3. The error bars represent one standard deviation, obtained in the fitting procedure. Since each experiment was performed on different occasions and the results were not normalized against each other they are not quantitative, only their trends are comparable. For comparison, Figure 7 displays the integrated intensity of the asymmetric COO^- vibration collected with IRAS for zinc exposed to dry and humid air containing formic acid. From Figure 6 it is clear that the VSFS amplitude of the formate stabilizes within approximately the same time, about 90 min, for both humid and dry exposures. The behavior of the VSFS amplitudes in Figure 6 is contrasted by the IRAS intensity (Figure 7), which continue to grow beyond 90 min of exposure in both dry and humid air. This dissimilarity can be explained by the difference in what the two techniques are probing; VSFS is surface sensitive, while IRAS obtains signals from the near-surface region.

The amplitudes extracted from the VSFS spectra are not easily quantified. They do not have a clear relationship with the number of formates at the surface; the amplitude depends on the ordering of the surface species as well as the number of molecules. A possible interpretation of the results could be that after 90 min exposure a thin film has formed with an ordered layer of formate on top, while the bulk formate is not seen because of a disordered or centrosymmetric structure. There is also the interface between the film and metal, which also could contribute to the signal, when the ZnO/Zn has been exposed long enough so that a thin film of Zn formate is present at the interface. Thin film systems have been studied with VSFS,[48,55] and the conclusion was that the total sum frequency signal was a convolution of the signal generated at the two interfaces. Therefore it is likely that also in this case the sum frequency signal gets contribution from both the metal/formate interface in addition to the formate/liquid interface.

Similar experiments, metal surfaces exposed to formic acid, have been performed with VSFS on Mg, Ni and Pt.[48−54] Here it was seen that interference in the thin film of Zn formate or formic acid caused the sum frequency amplitude to oscillate with exposure time. This is different from what is observed in Figure 6. The difference possibly originates from the fact that a polycrystalline sample was used here with a surface roughness

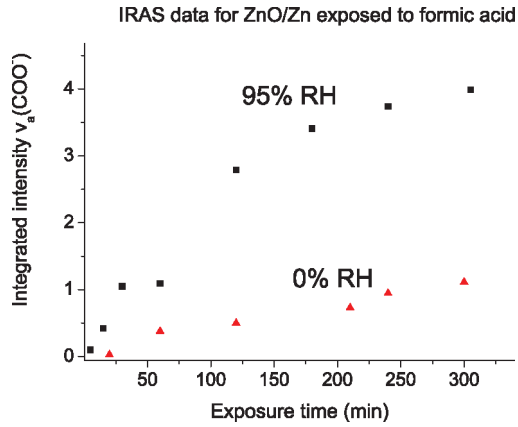

Figure 7. Growth of the antisymmetric COO^- peak, as monitored by IRAS, for ZnO/Zn exposed to humid or dry air and formic acid.

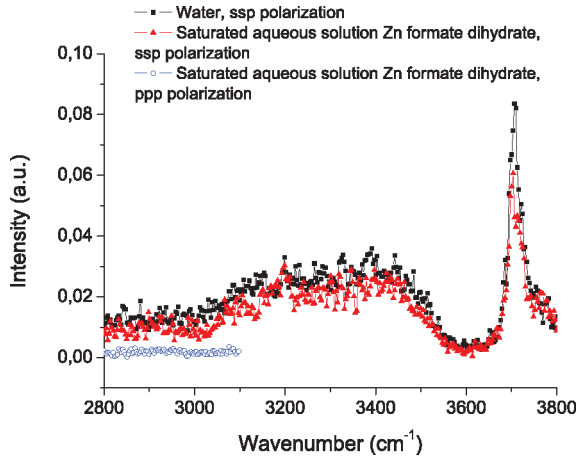

Figure 8. VSFS spectrum of air/liquid interface for pure water (filled squares) and saturated, aqueous solution of zinc formate dihydrate, ssp polarization (filled triangles), ppp polarization (open circles).

much greater than the single crystalline substrates used in the work mentioned. The roughness and heterogeneity will prohibit an interference pattern of the VSFS amplitude.

A stationary state is observed regarding the surface formate for exposures beyond 90 min in both humid and dry air, as seen in the stabilization of the VSFS amplitudes in Figure 6, yet the formate film continues to grow as seen with IRAS. Note that the amplitude of the asymmetric COO^- measured by IRAS is several times larger for exposures in humid air than in dry air containing formic acid, meaning that the growth rate of the thin film is markedly faster in humid air. The difference between the VSFS and IRAS results indicates that there are two different processes governing the growth of the thin film of formates, one which has little dependency on the water content (seen with VSFS), and one which definitely shows an acceleration with increased amount of water (seen with IRAS). This will be discussed in the next section.

General Interpretation of VSFS and IRAS Data. A model has recently been proposed for the initial atmospheric corrosion of zinc accelerated by carboxylic acids.[12] The model includes the deposition of the carboxylic acid into the aqueous adlayer and concomitant dissociation into a proton and carboxylate ion. The next steps is a ligand-exchange between the carboxylate ion or proton with surface hydroxyl groups, surface-coordination of the ligands with zinc, followed by ligand-induced dissolution of zinc ions and the precipitation of zinc carboxylate solid. The growth of multilayers is accelerated with increased water content on the surface.

The parallel results from IRAS and VSFS allow a comparison to be made between the nature of zinc-formate formed at the zinc surface and in the multilayers respectively. The IRAS results presented here have been published before as part of a study focusing on that technique, so details on these spectra have been omitted here.[2] Several pieces of evidence of the electrochemical nature of the corrosion processes involved were presented.[12] First, the significant sensitivity in growth kinetics with relative humidity of the humidified air, second, the fact that the growth kinetics was markedly reduced when changing from humidified air to humidified nitrogen gas, albeit the experiments on nitrogen gas were performed with acetaldehyde as corrosion accelerator. In addition the ZnO has been observed to be formed[15] through dissolved zinc ions liberated in the anodic reaction

$$Zn \rightarrow Zn^{2+} + 2e^- \quad (4)$$

and hydroxyl ions liberated in the cathodic reaction

$$^1/_2O_2 + 2e^- + H_2O \rightarrow 2OH^- \quad (5)$$

This is followed by precipitation of ZnO

$$Zn^{2+} + 2(OH)^- \rightarrow ZnO + H_2O \quad (6)$$

Current VSFS data, on the other hand, clearly show the same growth behavior of surface-formate species with or without humidity present in the air. Hence the process cannot be of electrochemical nature and suggest that the formates observed act as precursors for initial zinc dissolution, as discussed previously.[2,12] It is postulated that formate coordinated to zinc at the oxide surface weakens the zinc−oxygen bonds, whereby zinc dissolves into the aqueous adlayer and reprecipitates (as zinc formate) on the surface, thus exposing more metallic zinc. From this moment electrochemistry drives the atmospheric corrosion process through the Zn/Zn^{2+} and O_2/H_2O redox couples, whereby the corrosion rate increases with increasing thickness of the aqueous adlayer (relative humidity), which also becomes more pronounced with higher relative humidity.

Discussion on Studied Interfaces. As VSFS is a surface sensitive technique, there exists an issue of which interface the sum frequency generated beam originates from in these experiments (i.e., gas−liquid or liquid−solid). As the zinc surface is humidified a thin film of water is formed. Thus two interfaces are present: the metal-water and the air−water air interface. For long exposure times, where a thin film has formed on the surface, there is an additional interface: metal-formate. The possible contribution from this interface has been discussed previously. To elucidate if the air/water interface could contribute to the sum frequency signal, an experiment on an aqueous solution saturated with zinc formate dihydrate ($Zn(HCOO)_2 \cdot 2H_2O$) was conducted. Zinc formate is considered a suitable model system for this control experiment since it is of interest if the formate can order on the air/water interface and give rise to a sum frequency signal. The results showed no peaks in the CH-region for either ssp or ppp polarizations (see Figure 8). The features observed in Figure 8 are the broad spectral response from hydrogen-bonded water molecules (3100−3600 cm^{-1}) and the free OH of the same molecule at 3700 cm^{-1}. The appearance of the spectrum clearly resembled the pure water spectrum,[56] although with a slightly lower intensity. This concludes that if the air/water interface is probed in addition to the water/metal interface, there is no significant contribution to the spectrum from the air/liquid interface in the CH region (2800−3100 cm^{-1}), since the VSFS spectra of Zn exposed to formic acid in humid air show strong peaks in the CH region, as previously

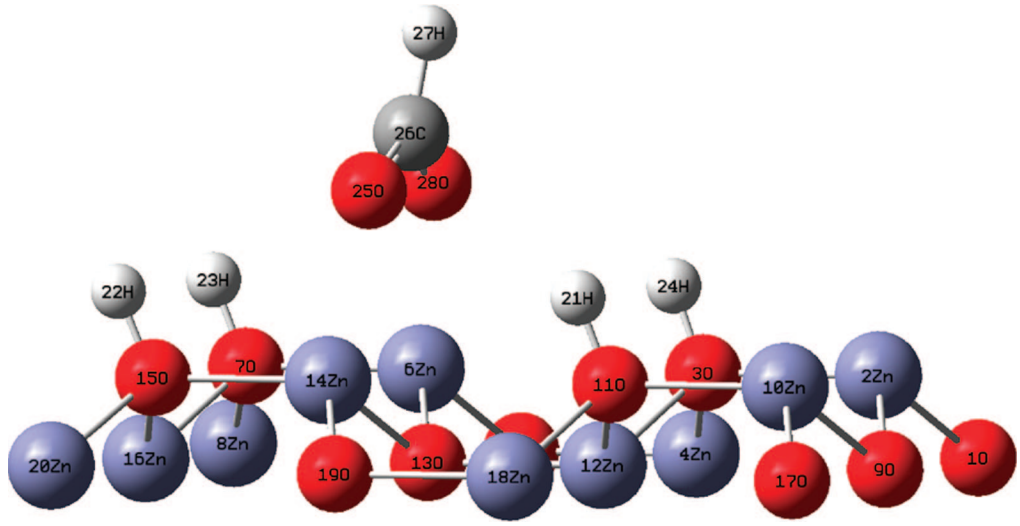

Figure 9. ZnO (100) cluster representation and a fully optimized hydroxylated layer upon interaction with a formate ion together with an implicit water solvate model.

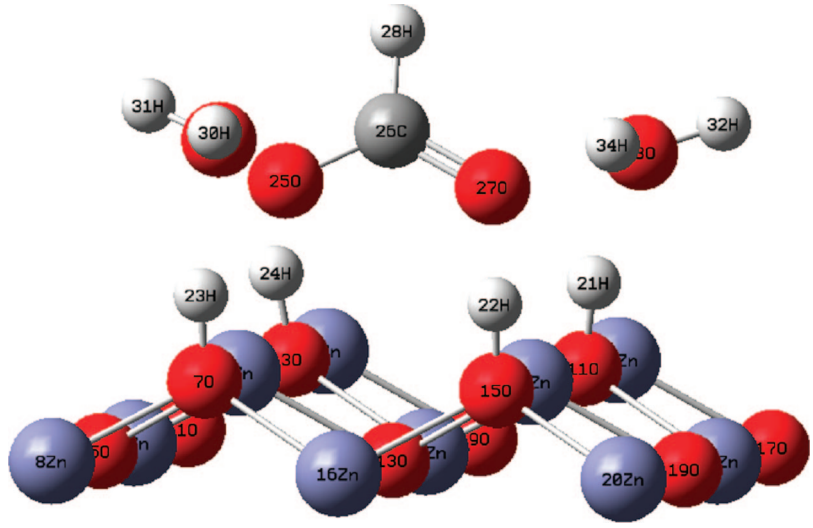

Figure 10. ZnO (100) cluster representation and a fully optimized hydroxylated layer upon interaction with a formate ion and two explicit water molecules together with an implicit water solvate model.

discussed. Thus VSFS in this experiment is an effective probe of the liquid−solid interface.

In all, the initial atmospheric corrosion of zinc induced by formic acid appears to involve both chemical (acid/base reaction) and electrochemical processes. The former governs the ligand-exchange and chemical dissolution of zinc, the latter governs subsequent atmospheric corrosion resulting in formation of multilayers of zinc-formate. In the section to follow, the nature of the interaction between the formate ion and the zinc oxide surface is further discussed by means of first principle calculations.

DFT Calculations. In the present section, an attempt is made to elucidate possible interactions between the formate ion and the zinc oxide surface during early stages of atmospheric corrosion and the influence of water molecules on the system by performing DFT calculations. The calculations are herein regarded as a complement to the VSFS results and interpretations. Figure 9 displays the resulting geometry based on calculations with the hydroxylated ZnO(100) surface interacting with one formate ion, in the presence of the implicit PCM solvate model. The most immediate conclusion is that the formate ion binds directly to the Zn^{2+} sites through two oxygen atoms, without any participation of hydrogen bonding originating from surface hydroxyl groups. A theoretical analysis of the vibrational frequencies of the optimized structure shows a frequency corresponding to the symmetric COO^- vibration, without any participation of surface hydroxyl groups on the formate-zinc adsorption process.

Figure 10 shows the system with the hydroxylated ZnO(100) surface interacting with one formate ion, two explicit water molecules, and with the PCM solvate model present. In the theoretical vibrational analysis no resonance peak appears which, is associated with coordination of the two water molecules to the hydroxylated layer. However, zinc-formate interaction shows a frequency signal at 1310 cm^{-1}, that indicates in this system the water molecules contribute very little to the adsorption process. In agreement with the VSFS data, the DFT calculations show a strong interaction between the formate and the zinc, and only minor participation from water molecules. A calculated frequency of ∼1310 cm^{-1} is observed, corresponding to direct interaction between the two oxygen atoms in the formate ion and two zinc atoms of the substrate.

Conclusions

In situ experiments were performed with VSFS on ZnO/Zn exposed to formic acid in combination with ab initio density

functional theory calculations have been performed in order to understand the first step of atmospheric corrosion initiated by formic acid. Also, infrared reflection absorption spectroscopy has been employed to complement the surface sensitive VSFS results with a near-surface probing technique.

The formic acid adsorption on zinc is seen to have a low dependency on the humidity, as deduced by VSFS. Zn formate is present on the surface in both dry and humid air and stabilizes in configuration after about 90 min exposure in 120 ppb formic acid as seen in the VSFS results. This is evidenced by the occurrence of the CH and symmetric COO^- vibrations of the formate ion.

From the analysis of the DFT studies it may be noted that the formate ion can interact with a hydroxylated ZnO cluster representation. The interaction takes place directly on the zinc atoms without any evident participation of hydroxylated layer and the formate ion adsorption does not vary greatly when water molecules are present. The theoretical analysis is in agreement with the VSFS experiments, where the results for exposures in humid and dry air have similar kinetics. The comparison between VSFS and IRAS results show that although the surface configuration is not changing, reactions are taking place and the film of corrosion products grows as seen by IRAS. The results from IRAS strongly show that a higher water content on the surface accelerates the growth of the layer of corrosion products involving formates.

In all, the combined results from VSFS, IRAS and DFT agree that the process by which the formic acid initiates the corrosion attack on the zinc surface is by a ligand-exchange process, where the formate is formed by deprotonation of formic acid. This reaction has a very low dependency on the water content on the surface. But the reaction governing the growth of the thin film of formates, seen with IRAS, has a high dependency on the water content.

Acknowledgment. J. Hedberg acknowledges the Swedish Research Council (VR) for financial support. J. Henriquez acknowledges projects ACT/24 and PBCT-PSD-16 of CONICYT-CHILE for the financial support. S. Baldelli acknowledges NSF (CHE-0650779) for funding.

References and Notes

(1) Aastrup, T.; Leygraf, C. *J. Electrochem. Soc.* **1997**, *144*, 2986.
(2) Johnson, C. M.; Leygraf, C. *J. Electrochem. Soc.* **2006**, *153*, B547.
(3) Persson, D.; Leygraf, C. *J. Electrochem. Soc.* **1995**, *142*, 1459.
(4) Persson, D.; Leygraf, C. *J. Electrochem. Soc.* **1995**, *142*, 1468.
(5) Niklasson, A; Johansson, L.-G; Svensson, J.-E. Proc. Met. 2004.
(6) Niklasson, A.; Johansson, L. G.; Svensson, J. E. *J. Electrochem. Soc.* **2007**, *154*, C618.
(7) Graedel, T. E. *J. Electrochem. Soc.* **1992**, *139*, 1963.
(8) Tyrode, E.; Johnson, C. M.; Leygraf, C. *Abstracts Papers Am. Chem. Soc.* **2005**, *230*, U2905.
(9) Johnson, C. M.; Tyrode, E.; Baldelli, S.; Rutland, M. W.; Leygraf, C. *J. Phys. Chem. B* **2005**, *109*, 321.
(10) Tyrode, E.; Johnson, C. M.; Baldelli, S.; Leygraf, C.; Rutland, M. W. *J. Phys. Chem. B* **2005**, *109*, 329.
(11) Gil, H.; Leygraf, C. *J. Electrochem. Soc.* **2007**, *154*, C272.
(12) Johnson, C. M.; Leygraf, C. *J. Electrochem. Soc.* **2006**, *153*, B542.
(13) *Encyclopedia of Electrochemistry*; Wiley VCH GmbH & Co, KGaA; Vol. 4.
(14) Evans, U. R. *The Corrosion and Oxidation of Metals*; Edward Arnold (Publishers) Ltd.: London, 1960.
(15) Svensson, J. E.; Johansson, L. G. *J. Electrochem. Soc.* **1993**, *140*, 2210.
(16) Guyotsionnest, P.; Hunt, J. H.; Shen, Y. R. *Phys. Rev. Lett.* **1987**, *59*, 1597.
(17) Shen, Y. R. *Nature* **1989**, *337*, 519.
(18) Greenler, R. G. *J. Phys. Chem.* **1969**, *50*, 1963.
(19) Frisch, M. J.; T., G. W.; Schlegel, H. B.; Scuseria, G. E.; Robb, M. A.; Cheeseman, J. R.; Montgomery, J. A., Jr.; Vreven, T.; Kudin, K. N.; Burant, J. C.; Millam, J. M.; Iyengar, S. S.; Tomasi, J.; Barone, V.; Mennucci, B.; Cossi, M.; Scalmani, G.; Rega, N.; Petersson, G. A.; Nakatsuji, H.; Hada, M.; Ehara, M.; Toyota, K.; Fukuda, R.; Hasegawa, J.; Ishida, M.; Nakajima, T.; Honda, Y.; Kitao, O.; Nakai, H.; Klene, M.; Li, X.; Knox, J. E.; Hratchian, H. P.; Cross, J. B.; Adamo, C.; Jaramillo, J.; Gomperts, R.; Stratmann, R. E.; Yazyev, O.; Austin, A. J.; Cammi, R.; Pomelli, C.; Ochterski, J. W.; Ayala, P. Y.; Morokuma, K.; Voth, G. A.; Salvador, P.; Dannenberg, J. J.; Zakrzewski, V. G.; Dapprich, S.; Daniels, A. D.; Strain, M. C.; Farkas, O.; Malick, D. K.; Rabuck, A. D.; Raghavachari, K.; Foresman, J. B.; Ortiz, J. V.; Cui, Q.; Baboul, A. G.; Clifford, S.; Cioslowski, J.; Stefanov, B. B.; Liu, G.; Liashenko, A.; Piskorz, P.; Komaromi, I.; Martin, R. L.; Fox, D. J.; Keith, T.; Al-Laham, M. A.; Peng, C. Y.; Nanayakkara, A.; Challacombe, M.; Gill, P. M. W.; Johnson, B.; Chen, W.; Wong, M. W.; Gonzalez, C. and Pople, J. A. *Gaussian 03* Gaussian, Inc.; Revision C.02 ed. Wallingford CT, 2004.
(20) Becke, A. D. *J. Chem. Phys.* **1993**, *98*, 5648.
(21) Lee, C. T.; Yang, W. T.; Parr, R. G. *Phys. Rev. B* **1988**, *37*, 785.
(22) Dunning, T. H., Jr; H., P. J. *Modern Theoretical Chemistry*; Plenum: New York, 1976; Vol. 3.
(23) Johnston, R. L. *Atomic and Molecular Clusters*; Johnston, R., Johnston, L., Eds.; CRC Press: Boca Raton, FL, 2002.
(24) Au, C. T.; Roberts, M. W.; Zhu, A. R. *Surf. Sci.* **1982**, *115*, L117.
(25) Barone, V.; Cossi, M.; Tomasi, J. *J. Chem. Phys.* **1997**, *107*, 3210.
(26) Matsumoto, T.; Bandara, A.; Kubota, J.; Hirose, C.; Domen, K. *J. Phys. Chem. B* **1998**, *102*, 2979.
(27) Mennucci, B.; Cances, E.; Tomasi, J. *J. Phys. Chem. B* **1997**, *101*, 10506.
(28) Mennucci, B.; Tomasi, J. *J. Chem. Phys.* **1997**, *106*, 5151.
(29) Miertus, S.; Scrocco, E.; Tomasi, J. *Chem. Phys.* **1981**, *55*, 117.
(30) Miertus, S.; Tomasi, J. *Chem. Phys.* **1982**, *65*, 239.
(31) Millar, G. J.; Rochester, C. H.; Waugh, K. C. *J. Chem. Soc., Faraday Trans.* **1992**, *88*, 1033.
(32) Nara, M.; Torii, H.; Tasumi, M. *J. Phys. Chem.* **1996**, *100*, 19812.
(33) Cimiraglia, R.; Persico, M.; Tomasi, J. *Chem. Phys. Lett.* **1980**, *76*, 169.
(34) http://www.nsc.liu.se/systems/monolith/.
(35) http://dta.utalca.cl/quimica/, h. c. u. c.
(36) Dennington, R. K., II; Millam, J. *GView*; 4.1 ed.; Semichem Inc.: Kansas City, 2007.
(37) Humphrey, W.; Dalke, A.; Schulten, K. *J. Mol. Graphics* **1996**, *14*, 33.
(38) Mikhailovsky, Y. N. *Theoretical and engineering principles of atmospheric corrosion of metals, Atmospheric Corrosion*; Wiley: New York, 1982; p 82.
(39) Crook, S.; Dhariwal, H.; Thornton, G. *Surf. Sci.* **1997**, *382*, 19.
(40) Davis, R.; Walsh, J. F.; Muryn, C. A.; Thornton, G.; Dhanak, V. R.; Prince, K. C. *Surf. Sci.* **1993**, *298*, L196.
(41) Johnson, C. M.; Tyrode, E.; Leygraf, C. *J. Electrochem. Soc.* **2006**, *153*, B113.
(42) Petrie, W. T.; Vohs, J. M. *Surf. Sci.* **1991**, *245*, 315.
(43) Ueno, A.; Onishi, T.; Tamaru, K. *Trans. Faraday Soc.* **1970**, *66*, 756.
(44) Noto, Y.; Fukuda, K.; Onishi, T.; Tamura, K. *Trans. Faraday Soc.* **1967**, *63*, 3081.
(45) Millikan, R. C.; Pitzer, K. S. *J. Am. Chem. Soc.* **1958**, *80*, 3515.
(46) Mikawa, Y.; Jakobsen, R. J.; Brasch, J. W. *J. Chem. Phys. Lett.* **1966**, *45*, 4751.
(47) Baradli, P. *Spectrochim. Acta* **1970**, *35A*, 1003.
(48) Hirose C., I. H.; Iwatsu, K.; Watanabe, N.; Kubota, J.; Wada, A.; Domen, K *J. Chem. Phys.* **1998**, *108*, 5948.
(49) Ishida, H.; Iwatsu, K.; Kubota, J.; Wada, A.; Domen, K.; Hirose, C. *J. Chem. Phys.* **1998**, *108*, 5957.
(50) Yamakata, A.; Kubota, J.; Kondo, J. N.; Hirose, C.; Domen, K.; Wakabayashi, F. *J. Phys. Chem. B* **1997**, *101*, 5177.
(51) Yamakata, A.; Kubota, J.; Kondo, J. N.; Hirose, C.; Domen, K.; Wakabayashi, F.; Tamaru, K. *J. Phys. Chem. B* **1998**, *102*, 4401.
(52) Yamamoto, H.; Watanabe, N.; Wada, A.; Domen, K.; Hirose, C. *J. Chem. Phys.* **1997**, *106*, 4734.
(53) Yuzawa, T.; Kubota, J.; Onda, K.; Wada, A.; Domen, K.; Hirose, C. *J. Mol. Struct.* **1997**, *413*, 307.
(54) Yuzawa, T.; Shioda, T.; Kubota, J.; Onda, K.; Wada, A.; Domen, K.; Hirose, C. *Surf. Sci.* **1998**, *416*, L1090.
(55) Holman, J.; Davies, P. B.; Nishida, T.; Ye, S.; Neivandt, D. J. *J. Phys. Chem. B* **2005**, *109*, 18723.
(56) Du, Q.; Superfine, R.; Freysz, E.; Shen, Y. R. *Phys. Rev. Lett.* **1993**, *70*, 2313.

JP805582H